

¹ **Supplementary Information for “Paleoclimate
2 pattern effects constrain climate sensitivity and
3 future warming”**

V. T. Cooper¹, K. C. Armour^{1,2}, G. J. Hakim¹, J. E. Tierney³, N. J. Burls⁴,
C. Proistosescu⁵, T. Andrews^{6,7}, W. Dong^{8,9}, M. T. Dvorak², R. Feng¹⁰, M.
B. Osman¹¹, Y. Dong¹²

⁴ ¹Department of Atmospheric and Climate Science, University of Washington, Seattle, WA, USA

⁵ ²School of Oceanography, University of Washington, Seattle, WA, USA

⁶ ³Department of Geosciences, University of Arizona, Tucson, AZ, USA

⁷ ⁴Department of Atmospheric, Oceanic and Earth Sciences, George Mason University, Fairfax, VA, USA

⁸ ⁵Department of Climate, Meteorology, and Atmospheric Sciences, University of Illinois at Urbana-Champaign, Champaign, IL, USA

⁹ ⁶Met Office Hadley Centre, Exeter, UK

¹⁰ ⁷School of Earth and Environment, University of Leeds, Leeds, UK

¹¹ ⁸Cooperative Programs for the Advancement of Earth System Science, University Corporation for Atmospheric Research, Boulder,
¹² CO, USA

¹³ ⁹NOAA/Geophysical Fluid Dynamics Laboratory, Princeton, NJ, USA

¹⁴ ¹⁰Department of Geosciences, University of Connecticut, Storrs, CT, USA

¹⁵ ¹¹Department of Geography, The University of Cambridge, Cambridge, UK

¹⁶ ¹²Department of Atmospheric and Oceanic Sciences, University of California Los Angeles, Los Angeles, CA, USA

¹⁷ **Contents of this file**¹⁸ 1. Figures S1 to S11¹⁹ 2. Tables S1 to S4

Corresponding author: Vincent T. Cooper, Department of Atmospheric and Climate Science,
University of Washington, Seattle, Washington, USA. (vcooper@uw.edu)

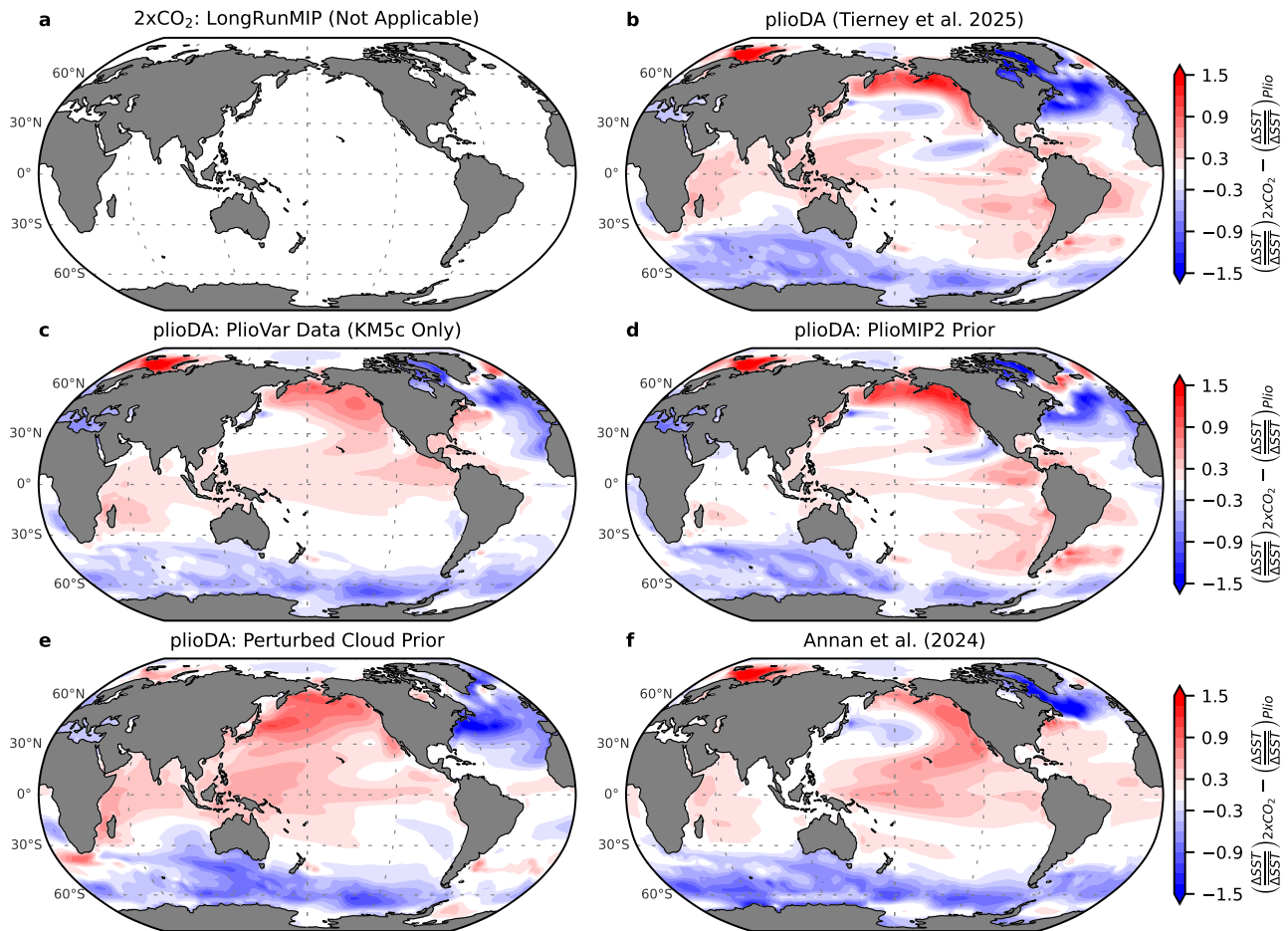


Figure S1. Differences between the 2xCO₂ pattern of sea-surface temperature (SST) anomalies and Pliocene patterns of SST anomalies. Panels correspond to Figure 1 of Main Text. Before taking the differences, each pattern's local anomalies are divided by its global-mean SST anomaly to emphasize the spatial patterns. Red regions indicate stronger relative amplification of warming in the LongRunMIP 2xCO₂ pattern (Rugenstein et al., 2019), while blue regions indicate stronger relative amplification of Pliocene warming. See Figure S10 for zonal-mean SST anomalies and pattern differences.

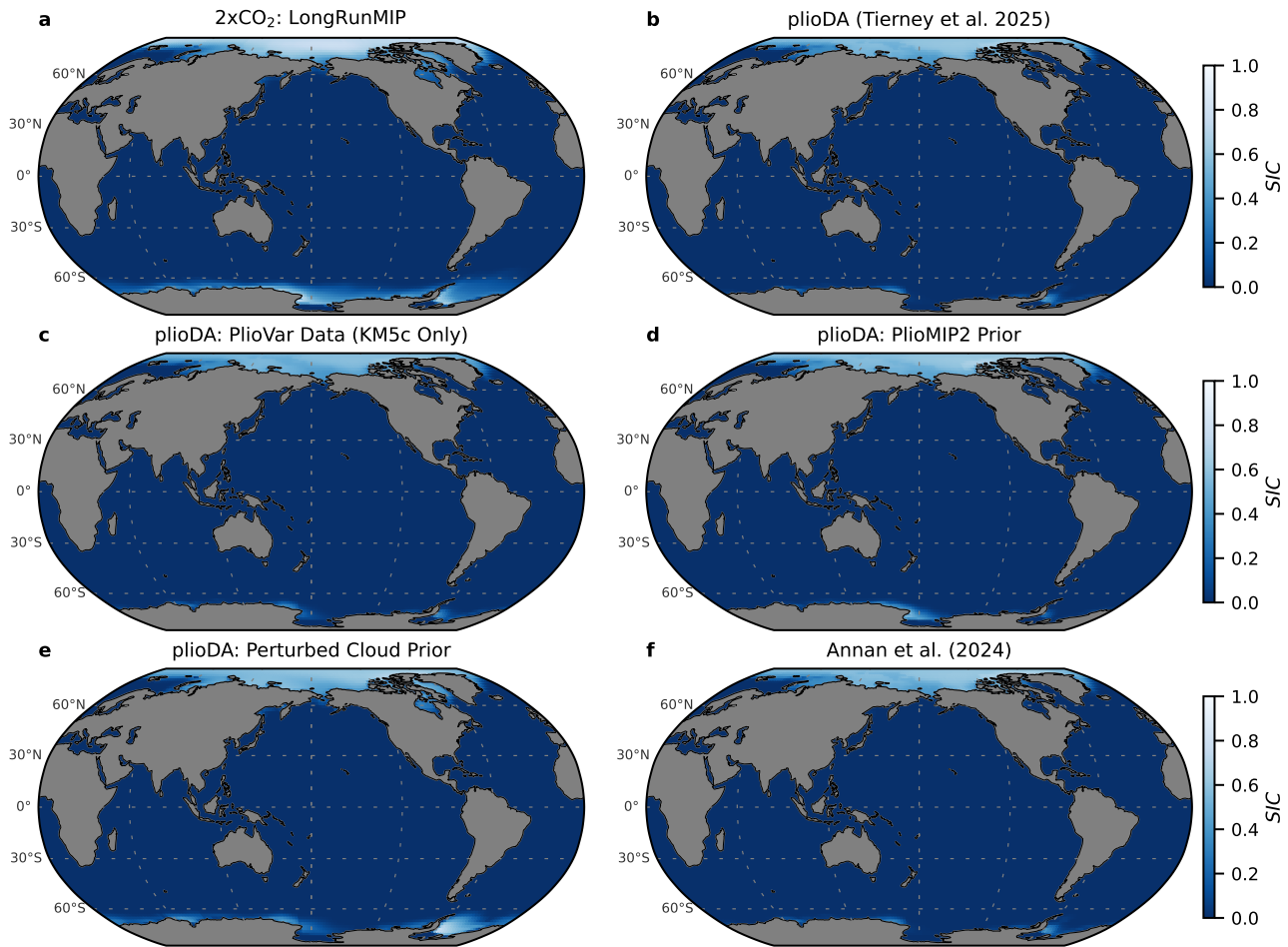


Figure S2. Sea-ice concentration (SIC): LongRunMIP 2xCO₂ and Pliocene reconstructions. Panels show annual-mean. Note that plioDA sea ice is used for the Annan et al. (2024) reconstruction.

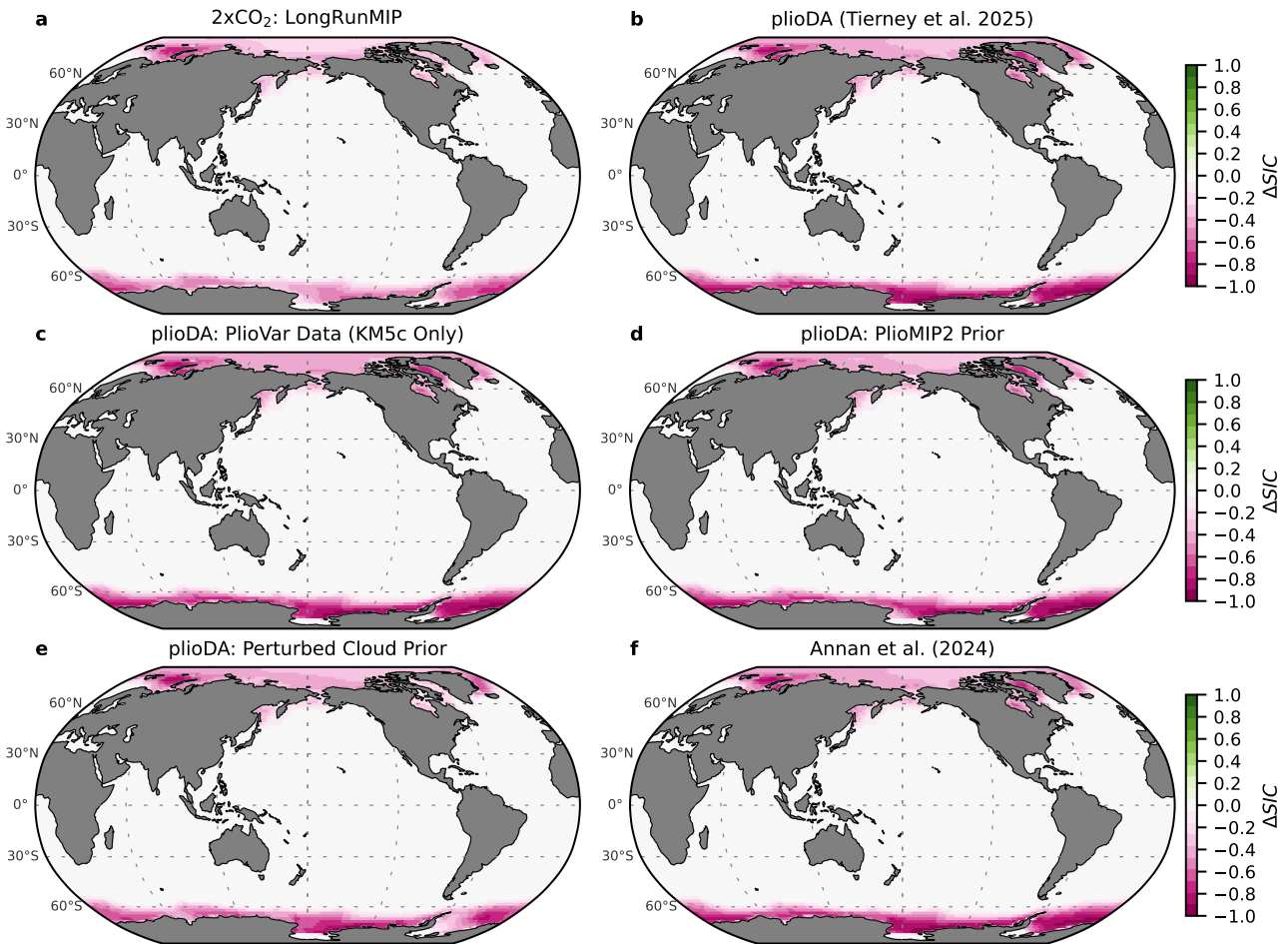


Figure S3. Sea-ice concentration (SIC) anomalies: LongRunMIP 2xCO₂ and Pliocene reconstructions relative to preindustrial baseline. Panels show annual-mean differences relative to the preindustrial (Late Holocene) baseline (Osman et al., 2021). Note that plioDA sea ice is used for the Annan et al. (2024) reconstruction.

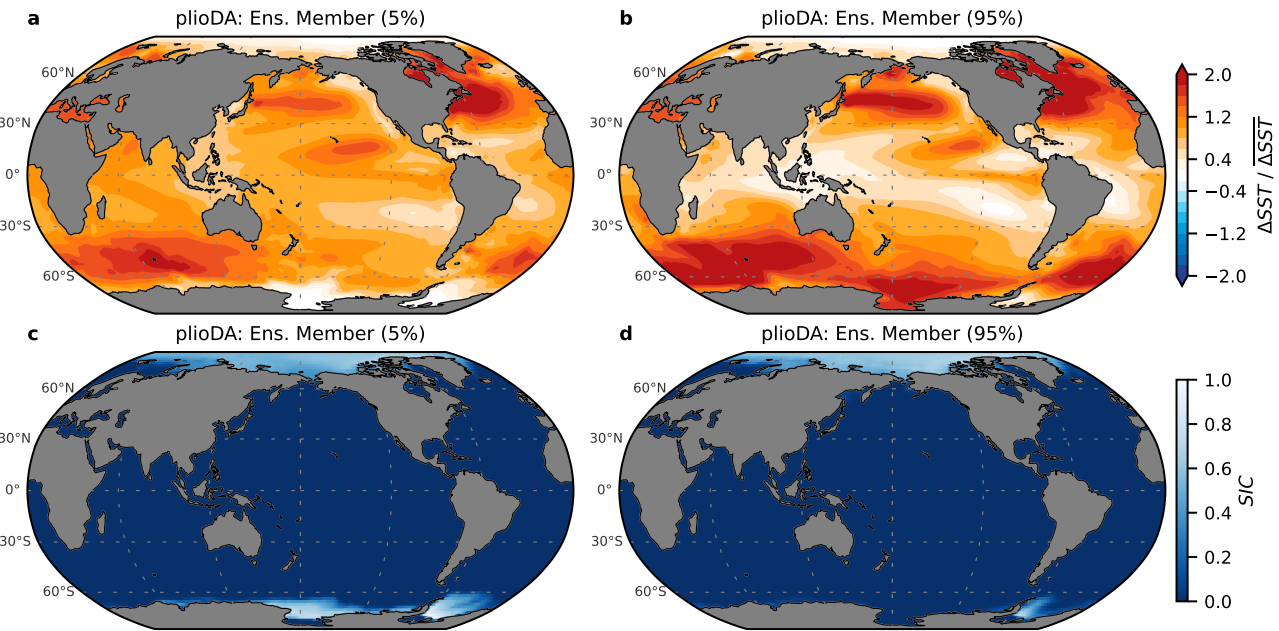


Figure S4. 5th and 95th percentile ensemble members from plioDA reconstruction (Tierney et al., 2025). (a–b) Sea-surface temperature (SST) anomalies and (c–d) sea-ice concentration (SIC) for ensemble members with the 5th percentile net feedback (more negative, stable climate) and 95th percentile net feedback (more positive, less stable climate). Ensemble members are ranked using CAM4 Green's functions (Dong et al., 2019).

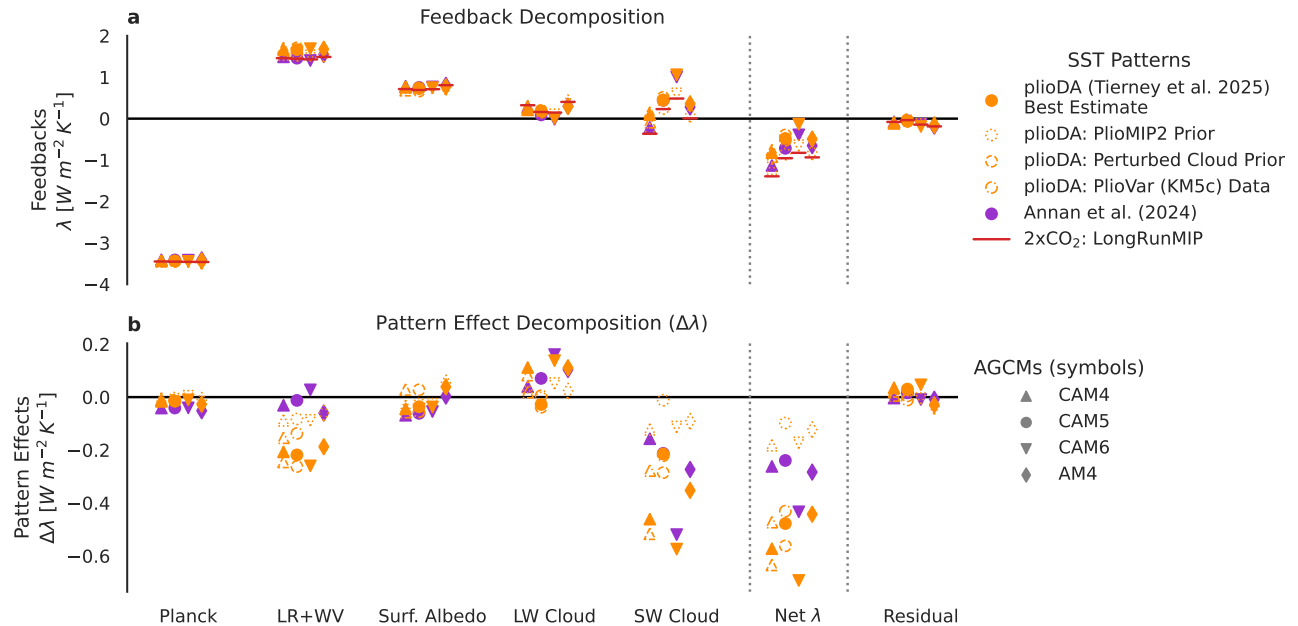


Figure S5. Kernel decomposition of radiative feedbacks (λ). Note that each legend applies to both panels: different sea-surface temperature and sea ice patterns are distinguished by colors/borders, while the different atmospheric general circulation models (AGCMs) are distinguished by symbol shapes. **(a)** Decomposition of feedbacks using radiative kernels (Soden et al., 2008) from CAM5 (Pendergrass et al., 2018). LR+WV represents the lapse rate and water vapor feedbacks. **(b)** Pattern effects ($\Delta\lambda = \lambda_{2xCO_2} - \lambda_{Plio}$) for each component feedback in panel a.

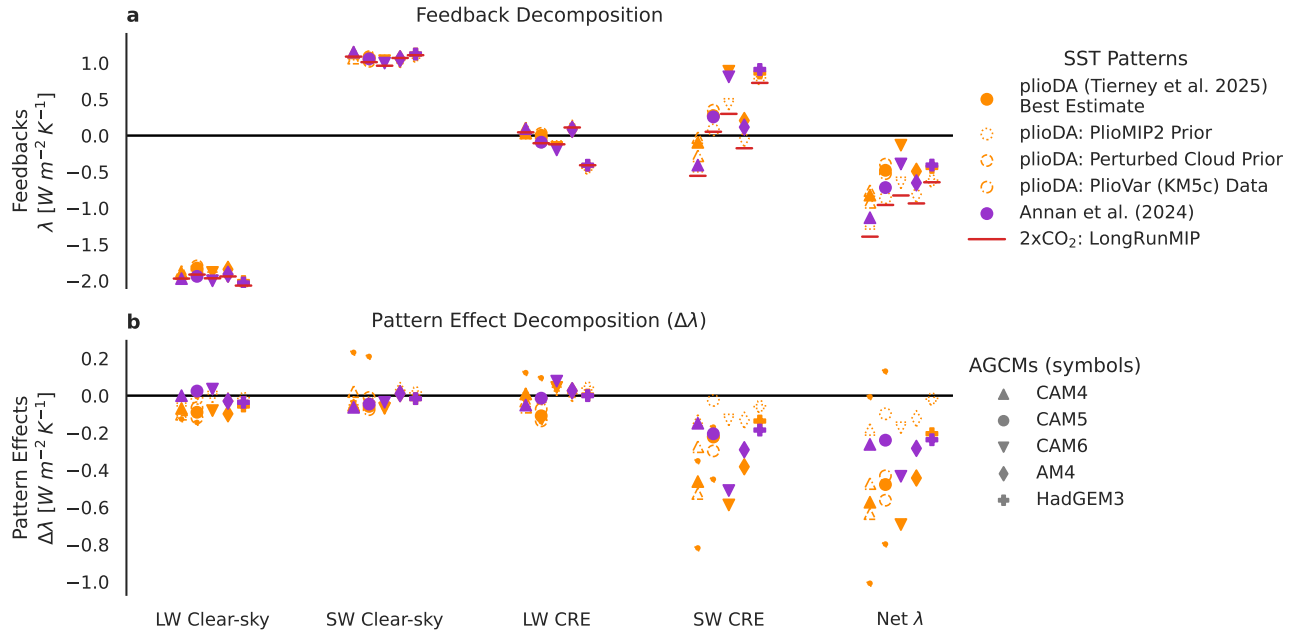


Figure S6. Decomposition of radiative feedbacks (λ) from direct model outputs for clear-sky radiation and cloud radiative effects (CRE). Results are separated into longwave (LW) and shortwave (SW) components. **(a)** Decomposition of feedbacks, and **(b)** decomposition of pattern effects ($\Delta\lambda = \lambda_{2xCO_2} - \lambda_{Plio}$).

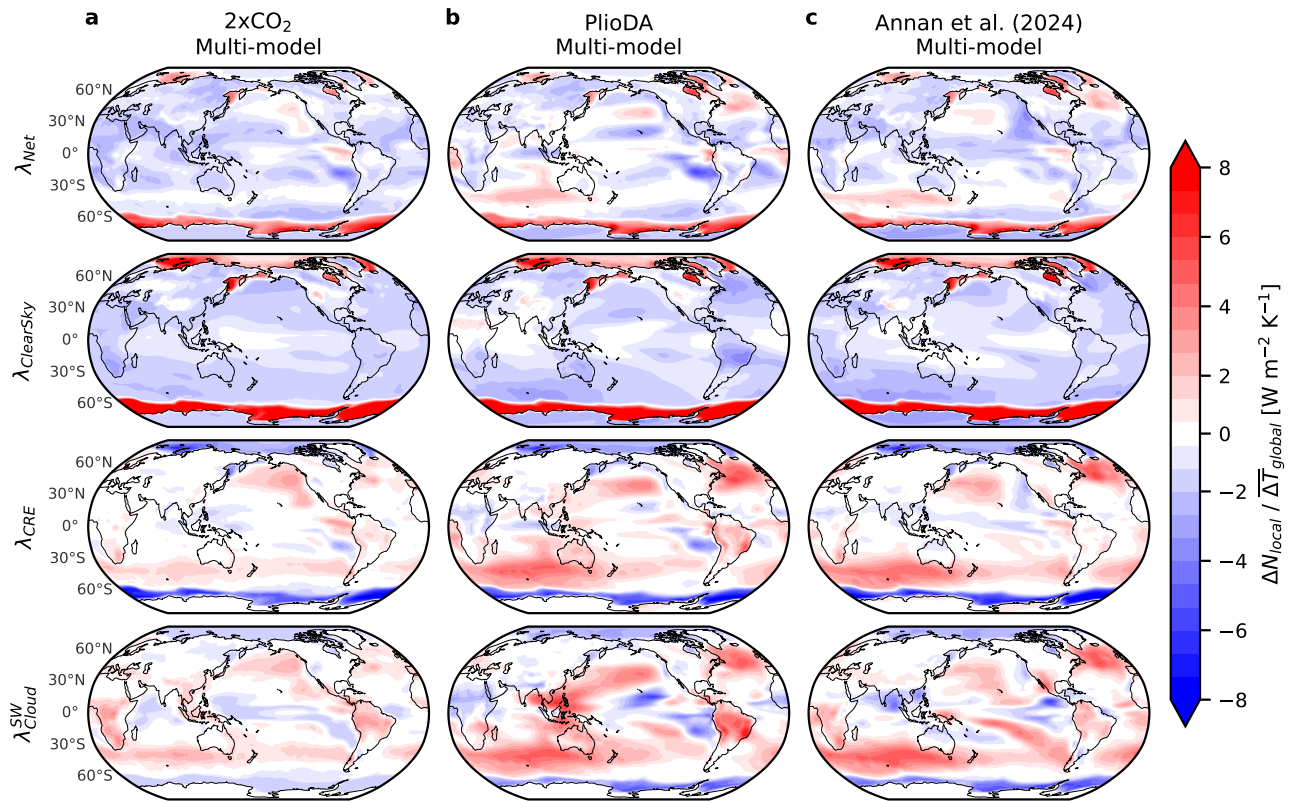


Figure S7. Spatial pattern of local radiative feedbacks (λ). Local feedbacks are calculated as $\Delta N / \overline{\Delta T}$, where ΔN is the local anomaly in top-of-atmosphere radiation, and $\overline{\Delta T}$ is the global-mean anomaly in near-surface air temperature. Multi-model mean, including CAM4, CAM5, CAM6, and GFDL-AM4 from (a) LongRunMIP 2xCO₂ (Rugenstein et al., 2019), (b) plioDA (Tierney et al., 2025), and (c) Annan et al. (2024).

20 **Figure S8–S9.** Zonal mean of local radiative feedbacks (λ) and pattern effects,
21 $\Delta\lambda = \lambda_{2xCO_2} - \lambda_{Plio}$, shown on the following pages. Local feedbacks are calculated as
22 $\Delta N/\overline{\Delta T}$, where ΔN is the local anomaly in top-of-atmosphere radiation, and $\overline{\Delta T}$ is the global-
23 mean anomaly in near-surface air temperature. **(a)** Feedbacks, λ , in CAM5 using various patterns
24 of sea-surface temperature (SST) and sea ice, and **(b)** Pattern effects, $\Delta\lambda = \lambda_{2xCO_2} - \lambda_{Plio}$, in
25 CAM5 corresponding to panel **a**. **(c–d)** Repeat of panels **a–b** with results from multiple models
26 (CAM4, CAM5, CAM6, and GFDL-AM4) and a subset of SST and sea ice patterns.

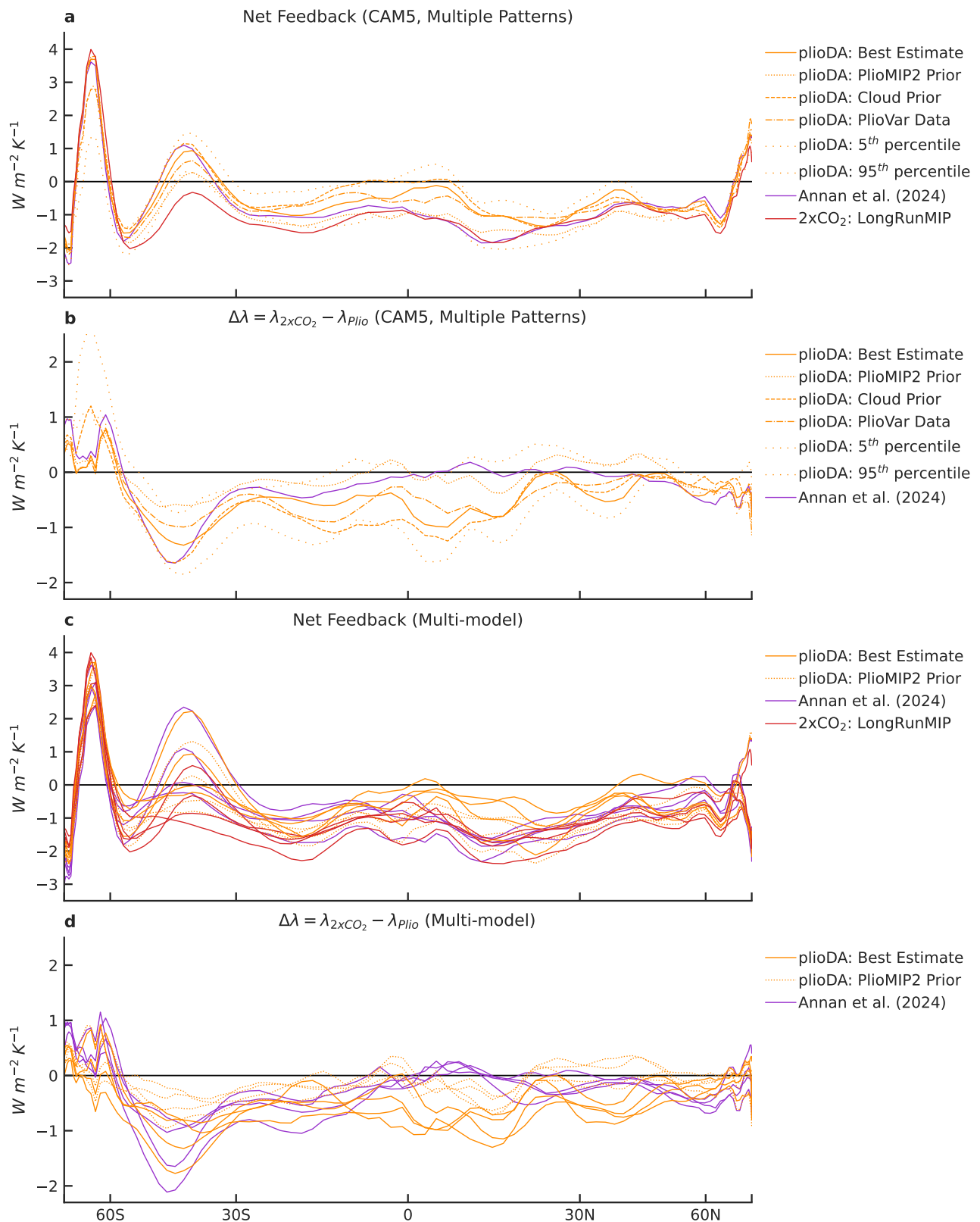


Figure S8. See caption on preceding page.

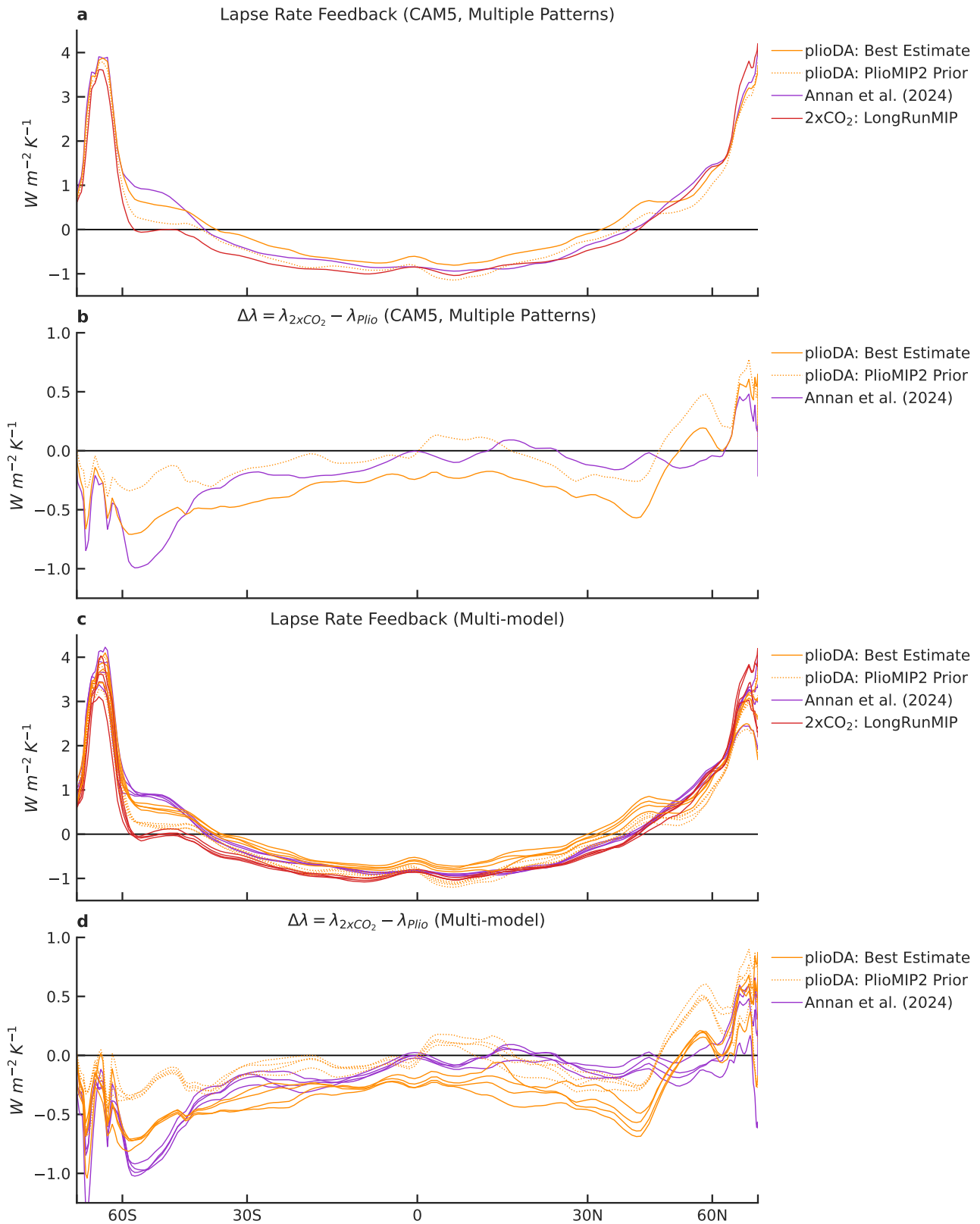


Figure S9. See caption that precedes Figure S8.

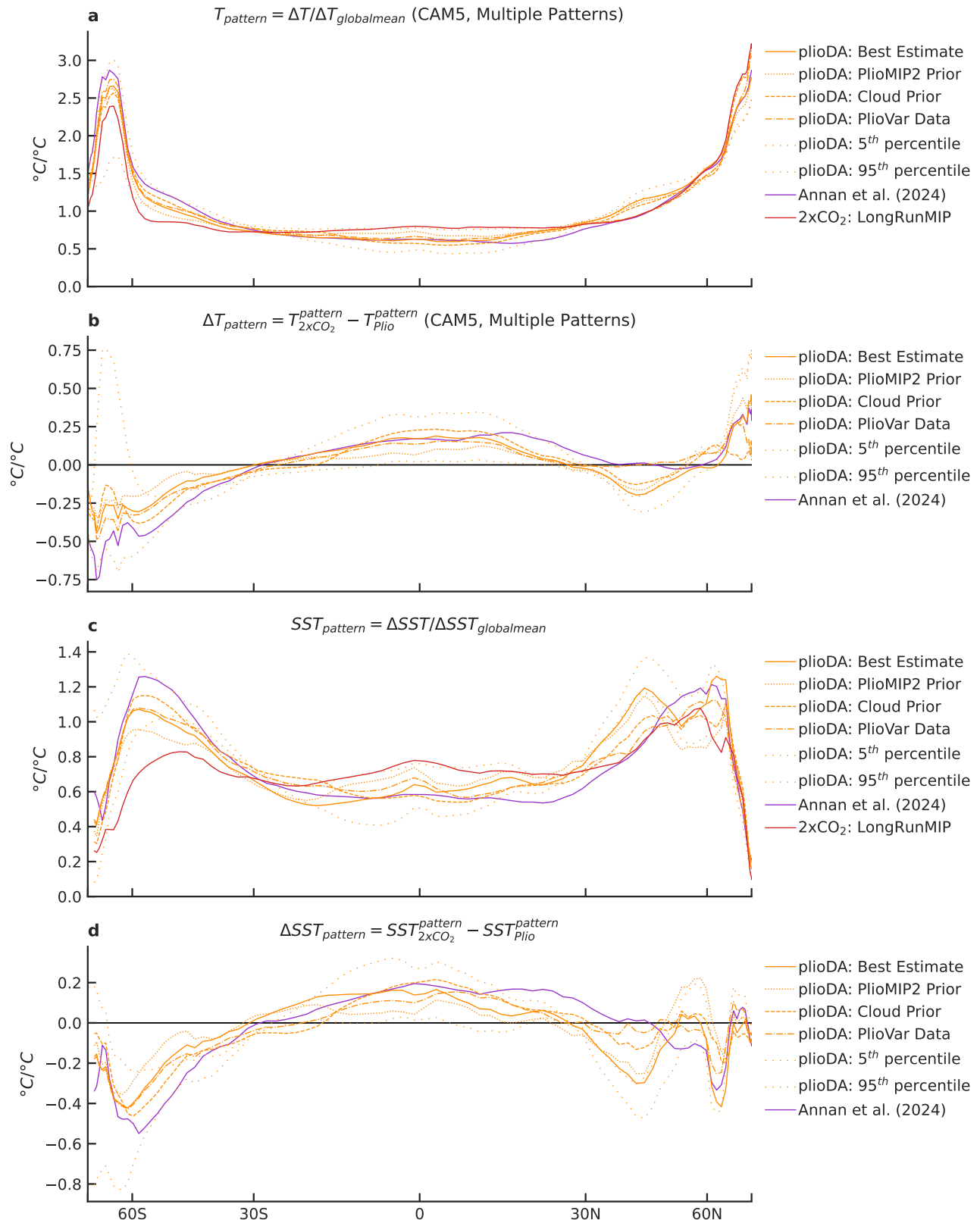


Figure S10. Zonal-mean patterns of temperature anomalies. (A) Normalized T from various patterns and (B) differences versus LongRunMIP 2xCO₂ pattern. (C–D) Repeats panels A and B for SST. Note that A–B show AGCM output from CAM5, whereas C–D show input boundary conditions for all AGCMs.

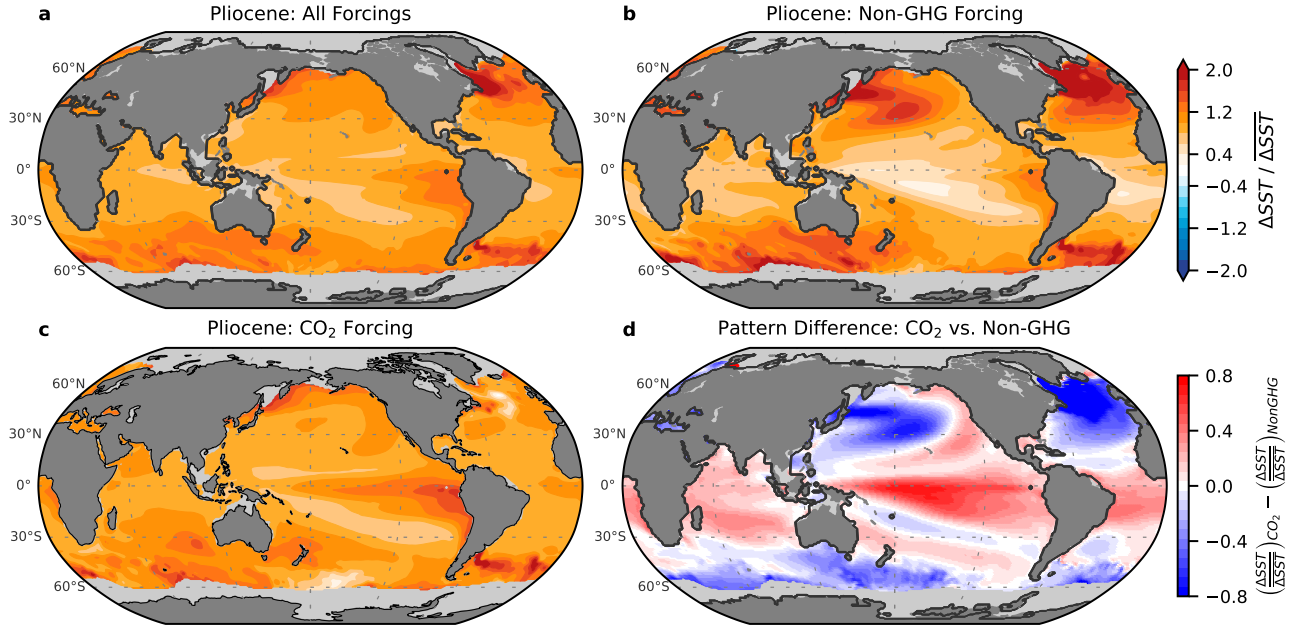


Figure S11. Sea-surface temperature (SST) response to Pliocene forcings in CESM2.1. Results shown are from (Dvorak et al., 2025). (a–c) Patterns of SST anomalies (normalized by global-mean anomalies) relative to preindustrial control from (a) all Pliocene forcings, (b) Non-GHG forcings including ice sheets, vegetation, topography, and bathymetry, and (c) CO₂ concentration of 400 ppm, which accounts for both CO₂ and methane forcing. (d) Difference between SST response to CO₂ versus non-GHG forcing, represented as panel c minus panel b; red regions indicate stronger relative amplification of warming from CO₂, while blue regions indicate stronger relative amplification from non-GHG forcings. In all panels, regions of preindustrial sea ice are masked in light gray. The CESM2 simulations follow the PlioMIP2 protocol (Haywood et al., 2020; Feng et al., 2022).

Table S1. All units are $\text{W m}^{-2} \text{ K}^{-1}$. Pliocene pattern effects, $\Delta\lambda = \lambda_{2x\text{CO}_2} - \lambda_{\text{Plio}}$, from three patterns of reconstructed Pliocene SST and sea ice in various AGCMs (CAM4 coupled to CLM4.5, CAM5.3 coupled to CLM5.0, CAM6.0 coupled to CLM5.0, GFDL-AM4.0, and HadGEM3-GC3.1-LL). Alternate values for Pliocene pattern effects, $\Delta\lambda_{150\text{yr}}^{\text{Alt}} = \lambda_{150\text{yr}}^{\text{CO}_2} - \lambda_{\text{Plio}}$, are shown using 150-yr regression of abrupt-4xCO₂ simulations (abrupt-2xCO₂ is used for CESM2-CAM6 to avoid issues with the ice nucleation scheme and cloud microphysics timestep that impact the feedback diagnosed from the 4xCO₂ simulation (Zhu et al., 2022; Burls & Sagoo, 2022)) from coupled models corresponding to each AGCM (Andrews et al., 2022).

Model	Pattern	$\Delta\lambda$	λ_{Plio}	$\lambda_{2x\text{CO}_2}$	$\Delta\lambda_{150\text{yr}}^{\text{Alt}}$	$\lambda_{150\text{yr}}^{\text{CO}_2}$
CAM4	plioDA	-0.57	-0.82	-1.39	-0.41	-1.23
CAM4	plioDA: PlioMIP2 Prior	-0.18	-1.21	-1.39	-0.02	-1.23
CAM4	Annan24	-0.26	-1.13	-1.39	-0.10	-1.23
CAM5	plioDA	-0.48	-0.48	-0.96	-0.67	-1.15
CAM5	plioDA: PlioMIP2 Prior	-0.10	-0.86	-0.96	-0.29	-1.15
CAM5	Annan24	-0.24	-0.72	-0.96	-0.43	-1.15
CAM6	plioDA	-0.69	-0.13	-0.83	-1.08	-1.21
CAM6	plioDA: PlioMIP2 Prior	-0.17	-0.65	-0.83	-0.56	-1.21
CAM6	Annan24	-0.43	-0.39	-0.83	-0.82	-1.21
GFDL-AM4	plioDA	-0.44	-0.49	-0.93	-0.37	-0.86
GFDL-AM4	plioDA: PlioMIP2 Prior	-0.12	-0.81	-0.93	-0.05	-0.86
GFDL-AM4	Annan24	-0.28	-0.65	-0.93	-0.21	-0.86
HadGEM3	plioDA	-0.20	-0.44	-0.64	-0.19	-0.63
HadGEM3	plioDA: PlioMIP2 Prior	-0.02	-0.62	-0.64	-0.01	-0.63
HadGEM3	Annan24	-0.24	-0.41	-0.64	-0.22	-0.63
CAM4	mean	-0.34	-1.05	-1.39	-0.18	-1.23
CAM5	mean	-0.27	-0.68	-0.96	-0.47	-1.15
CAM6	mean	-0.43	-0.39	-0.83	-0.82	-1.21
GFDL-AM4	mean	-0.28	-0.65	-0.93	-0.21	-0.86
HadGEM3	mean	-0.15	-0.49	-0.64	-0.14	-0.63
mean	Annan24	-0.29	-0.66	-0.95	-0.36	-1.02
mean	plioDA	-0.48	-0.47	-0.95	-0.54	-1.02
mean	plioDA: PlioMIP2 Prior	-0.12	-0.83	-0.95	-0.18	-1.02
mean	mean	-0.30	-0.65	-0.95	-0.36	-1.02
1σ	1σ		0.19	0.29		0.31

Table S2. Pliocene pattern effects, $\Delta\lambda = \lambda_{2xCO_2} - \lambda_{Plio}$, from various patterns of reconstructed Pliocene SST and sea ice in CAM4 and CAM5. Global-mean anomalies for SST, near-surface air temperature (T), and top-of-atmosphere radiative imbalance (N) are shown for reference. Alternate values for Pliocene pattern effects, $\Delta\lambda_{150\text{yr}}^{\text{Alt}} = \lambda_{150\text{yr}}^{\text{CO}_2} - \lambda_{Plio}$, are shown using 150-yr regression feedbacks (Table S1).

Model	Pattern	$\Delta\lambda$	λ	ΔSST	ΔT	ΔN	$\Delta\lambda_{150\text{yr}}^{\text{Alt}}$
		$\text{Wm}^{-2}\text{K}^{-1}$	$\text{Wm}^{-2}\text{K}^{-1}$	K	K	Wm^{-2}	$\text{Wm}^{-2}\text{K}^{-1}$
CAM4	plioDA	-0.57	-0.82	3.00	3.90	-3.20	-0.41
CAM4	plioDA: PlioVar Data	-0.47	-0.92	2.89	3.78	-3.48	-0.31
CAM4	plioDA: PlioMIP2 Prior	-0.18	-1.21	2.94	3.86	-4.67	-0.02
CAM4	plioDA: Cloud Prior	-0.63	-0.76	2.83	3.68	-2.79	-0.47
CAM4	plioDA: 5%	-0.01	-1.39	3.96	4.88	-6.77	0.16
CAM4	plioDA: 95%	-1.01	-0.38	3.29	4.02	-1.55	-0.85
CAM4	Annan24	-0.26	-1.13	2.82	3.72	-4.21	-0.10
CAM4 mean		-0.45	-0.94	3.10	3.98	-3.81	-0.29
CAM4 1σ		0.33	0.33	0.41	0.41	1.65	0.33
CAM4	<i>2xCO₂: LongRunMIP</i>		-1.39	2.35	3.16	-4.40	
CAM5	plioDA	-0.48	-0.48	3.00	3.98	-1.90	-0.67
CAM5	plioDA: PlioVar Data	-0.43	-0.53	2.89	3.85	-2.02	-0.62
CAM5	plioDA: PlioMIP2 Prior	-0.10	-0.86	2.94	3.96	-3.40	-0.29
CAM5	plioDA: Cloud Prior	-0.56	-0.39	2.83	3.75	-1.48	-0.76
CAM5	plioDA: 5%	0.13	-1.09	3.96	4.99	-5.42	-0.06
CAM5	plioDA: 95%	-0.80	-0.16	3.29	4.10	-0.65	-0.99
CAM5	Annan24	-0.24	-0.72	2.82	3.78	-2.71	-0.43
CAM5 mean		-0.35	-0.60	3.10	4.06	-2.51	-0.55
CAM5 1σ		0.31	0.31	0.41	0.43	1.55	0.31
CAM5	<i>2xCO₂: LongRunMIP</i>		-0.96	2.35	3.21	-3.07	

Table S3. Posterior distributions of climate sensitivity (S). “Combined Evidence” assumes the Baseline Prior, $\lambda \sim \text{Unif}(-10, 10) \text{ W m}^{-2} \text{ K}^{-1}$, and includes Process Understanding, Historical Evidence, and Paleoclimate Evidence from the Last Glacial Maximum (LGM) and Pliocene. The Robust Range also combines lines of evidence but assumes a Uniform S Prior, $S \sim \text{Unif}(0, 20) \text{ K}$ (Sherwood et al., 2020). “Pliocene Only” considers only Pliocene evidence and assumes the Uniform S Prior. All uncertainties shown are 1σ values. Table structure is comparable to Table 10 of Sherwood et al. (2020).

Combined Evidence (Baseline Prior)	5th	17th	50th	83rd	95th	Mean	ΔT_{Plio}	ΔF_{NonGHG}^{Plio}	ΔT_{LGM}
SW20: Original	2.3	2.6	3.1	3.9	4.7	3.2	3.0 ± 1.0	f_{ESS}	-5 ± 1
+ Update ΔT_{LGM}	2.3	2.7	3.2	4.1	5.0	3.4	3.0 ± 1.0	f_{ESS}	-6 ± 1
+ Update ΔT_{Plio}	2.6	2.9	3.6	4.6	5.6	3.8	4.1 ± 0.6	f_{ESS}	-6 ± 1
+ Update ΔF_{NonGHG}^{Plio}	2.5	2.8	3.4	4.3	5.2	3.6	4.1 ± 0.6	1.7 ± 1.0	-6 ± 1
Include only LGM $\Delta\lambda$	2.3	2.6	3.0	3.7	4.4	3.2	4.1 ± 0.6	1.7 ± 1.0	-6 ± 1
Include only Pliocene $\Delta\lambda$	2.3	2.6	3.1	3.9	4.7	3.3	4.1 ± 0.6	1.7 ± 1.0	-6 ± 1
Full Update incl. Paleo $\Delta\lambda$	2.1	2.4	2.8	3.4	4.0	2.9	4.1 ± 0.6	1.7 ± 1.0	-6 ± 1
Alt. Update incl. Paleo $\Delta\lambda_{150\text{yr}}^{\text{Alt}}$	2.1	2.4	2.8	3.5	4.1	3.0	4.1 ± 0.6	1.7 ± 1.0	-6 ± 1

Combined, Robust Range (Unif. S Prior)	5th	17th	50th	83rd	95th	Mean	ΔT_{Plio}	ΔF_{NonGHG}^{Plio}	ΔT_{LGM}
SW20: Original Robust Range (Unif. S)	2.4	2.8	3.5	4.5	5.7	3.7	3.0 ± 1.0	f_{ESS}	-5 ± 1
+ Update ΔT , ΔF_{NonGHG}^{Plio} (Unif. S)	2.6	3.0	3.8	4.9	6.2	4.0	4.1 ± 0.6	1.7 ± 1.0	-6 ± 1
Full Update incl. Paleo $\Delta\lambda$ (Unif. S)	2.3	2.6	3.1	3.8	4.6	3.2	4.1 ± 0.6	1.7 ± 1.0	-6 ± 1
Alt. Update incl. Paleo $\Delta\lambda_{150\text{yr}}^{\text{Alt}}$ (Unif. S)	2.3	2.6	3.1	3.9	4.8	3.3	4.1 ± 0.6	1.7 ± 1.0	-6 ± 1

Pliocene Only (Unif. S Prior)	5th	17th	50th	83rd	95th	Mean	ΔT_{Plio}	ΔF_{NonGHG}^{Plio}
SW20: Original	1.6	2.4	4.0	6.8	10.1	4.7	3.0 ± 1.0	f_{ESS}
+ Update ΔT_{Plio}	2.9	3.8	5.6	8.6	12.3	6.3	3.0 ± 1.0	f_{ESS}
+ Update ΔF_{NonGHG}^{Plio}	2.5	3.2	4.7	7.4	11.2	5.4	4.1 ± 0.6	1.7 ± 1.0
Include Pliocene $\Delta\lambda$	1.9	2.4	3.8	7.2	12.9	5.0	4.1 ± 0.6	1.7 ± 1.0
Alt. Pliocene $\Delta\lambda_{150\text{yr}}^{\text{Alt}}$	1.8	2.4	3.8	8.3	14.8	5.3	4.1 ± 0.6	1.7 ± 1.0

Units in $^{\circ}\text{C}$; ΔF units in W m^{-2} .

Table S4. Paired estimates of Pliocene and LGM pattern effects, which use similar methods for data assimilation and the same AGCMs. The pairs are used to estimate the Pearson correlation and covariance between estimates of Pliocene and LGM pattern effects (Cooper et al., 2024). For the standard $\Delta\lambda, r = 0.56$ and $\text{cov} = 0.0123 [\text{W m}^{-2} \text{K}^{-1}]^2$. For $\Delta\lambda_{150\text{yr}}^{\text{Alt}}, r = 0.87$ and $\text{cov} = 0.0562 [\text{W m}^{-2} \text{K}^{-1}]^2$. Table units are $\text{W m}^{-2} \text{K}^{-1}$. LGM results use updated CESM2.1 $\lambda_{150\text{yr}}^{\text{Alt}}$ in Table S1.

AGCM	Plio Pattern	LGM Pattern	$\Delta\lambda_{\text{Plio}}$	$\Delta\lambda_{\text{LGM}}$	$\Delta\lambda_{\text{Plio}}^{\text{Alt150}}$	$\Delta\lambda_{\text{LGM}}^{\text{Alt150}}$
CAM4	plioDA	LGMR	-0.57	-0.45	-0.41	-0.21
CAM5	plioDA	LGMR	-0.48	-0.31	-0.67	-0.41
CAM6	plioDA	LGMR	-0.69	-0.63	-1.08	-1.02
AM4	plioDA	LGMR	-0.44	-0.33	-0.37	-0.27
HadGEM3	plioDA	LGMR	-0.20	-0.27	-0.19	-0.29
CAM4	Annan	Annan	-0.57	-0.29	-0.10	-0.06
CAM5	Annan	Annan	-0.48	-0.09	-0.43	-0.18
CAM4	plioDA: Cloud Prior	LGMR	-0.63	-0.45	-0.47	-0.21
CAM5	plioDA: Cloud Prior	LGMR	-0.56	-0.31	-0.76	-0.41
CAM4	plioDA: Cloud Prior	lgmDA	-0.63	-0.69	-0.47	-0.45
CAM5	plioDA: Cloud Prior	lgmDA	-0.56	-0.51	-0.76	-0.61
CAM4	plioDA	lgmDA	-0.57	-0.69	-0.41	-0.45
CAM5	plioDA	lgmDA	-0.48	-0.51	-0.67	-0.61

References

- 27 Andrews, T., Bodas-Salcedo, A., Gregory, J. M., Dong, Y., Armour, K. C., Paynter, D., ...
28 Liu, C. (2022, 9). On the Effect of Historical SST Patterns on Radiative Feedback. *Journal*
29 *of Geophysical Research: Atmospheres*, 127(18). Retrieved from <https://onlinelibrary.wiley.com/doi/10.1029/2022JD036675> doi: 10.1029/2022JD036675
30
31 Annan, J. D., Hargreaves, J. C., Mauritsen, T., McClymont, E., & Ho, S. L. (2024, 9). Can we
32 reliably reconstruct the mid-Pliocene Warm Period with sparse data and uncertain models?
33 *Climate of the Past*, 20(9), 1989–1999. Retrieved from <https://cp.copernicus.org/articles/20/1989/2024/> doi: 10.5194/cp-20-1989-2024
34
35 Burls, N., & Sagoo, N. (2022, 12). Increasingly Sophisticated Climate Models Need the
36 Out-Of-Sample Tests Paleoclimates Provide. *Journal of Advances in Modeling Earth*
37 *Systems*, 14(12). Retrieved from <https://agupubs.onlinelibrary.wiley.com/doi/10.1029/2022MS003389> doi: 10.1029/2022MS003389
38
39 Cooper, V. T., Armour, K. C., Hakim, G. J., Tierney, J. E., Osman, M. B., Proistosescu, C., ...
40 Chmielowiec, P. (2024, 4). Last Glacial Maximum pattern effects reduce climate sensitivity
41 estimates. *Science Advances*, 10(16), 9461. Retrieved from <https://www.science.org/doi/10.1126/sciadv.adk9461> doi: 10.1126/sciadv.adk9461
42
43 Dong, Y., Proistosescu, C., Armour, K. C., & Battisti, D. S. (2019, 9). Attributing Historical
44 and Future Evolution of Radiative Feedbacks to Regional Warming Patterns using a Green's
45 Function Approach: The Preeminence of the Western Pacific. *Journal of Climate*, 32(17),
46 5471–5491. Retrieved from <https://journals.ametsoc.org/view/journals/clim/32/17/jcli-d-18-0843.1.xml> doi: 10.1175/JCLI-D-18-0843.1
47

- 48 Dvorak, M., Armour, K., Feng, R., Cooper, V., Zhu, J., Proistosescu, C., & Burls, N.
49 (2025). Mid-Pliocene climate forcing, sea-surface temperature patterns, and implica-
50 tions for modern-day climate sensitivity. *Journal of Climate (in press)*.. Retrieved from
51 https://vtcooper.github.io/files/papers/Dvorak_Pliocene_JCli_accepted.pdf
- 52 Feng, R., Bhattacharya, T., Otto-Bliesner, B. L., Brady, E. C., Haywood, A. M., Tindall,
53 J. C., ... Peltier, W. R. (2022, 3). Past terrestrial hydroclimate sensitivity controlled by
54 Earth system feedbacks. *Nature Communications*, 13(1), 1306. Retrieved from <https://www.nature.com/articles/s41467-022-28814-7> doi: 10.1038/s41467-022-28814-7
- 55 Haywood, A. M., Tindall, J. C., Dowsett, H. J., Dolan, A. M., Foley, K. M., Hunter, S. J., ...
56 Lunt, D. J. (2020, 11). The Pliocene Model Intercomparison Project Phase 2: large-scale
57 climate features and climate sensitivity. *Climate of the Past*, 16(6), 2095–2123. Retrieved
58 from <https://cp.copernicus.org/articles/16/2095/2020/> doi: 10.5194/cp-16-2095
59 -2020
- 60 Osman, M. B., Tierney, J. E., Zhu, J., Tardif, R., Hakim, G. J., King, J., & Poulsen,
61 C. J. (2021, 11). Globally resolved surface temperatures since the Last Glacial Maxi-
62 mum. *Nature*, 599(7884), 239–244. Retrieved from <https://www.nature.com/articles/s41586-021-03984-4> doi: 10.1038/s41586-021-03984-4
- 63 Pendergrass, A. G., Conley, A., & Vitt, F. M. (2018). Surface and top-of-atmosphere radiative
64 feedback kernels for CESM-CAM5. *Earth Syst. Sci. Data*, 10, 317–324. Retrieved from
65 <https://doi.org/10.5194/essd-10-317-2018> doi: 10.5194/essd-10-317-2018
- 66 Rugenstein, M., Bloch-Johnson, J., Abe-Ouchi, A., Andrews, T., Beyerle, U., Cao, L., ... Yang,
67 S. (2019, 12). LongRunMIP: Motivation and Design for a Large Collection of Millennial-

- Length AOGCM Simulations. *Bulletin of the American Meteorological Society*, 100(12), 2551–2570. Retrieved from <https://journals.ametsoc.org/view/journals/bams/100/12/bams-d-19-0068.1.xml> doi: 10.1175/BAMS-D-19-0068.1
- Sherwood, S. C., Webb, M. J., Annan, J. D., Armour, K. C., Forster, P. M., Hargreaves, J. C., ... Zelinka, M. D. (2020, 12). An Assessment of Earth's Climate Sensitivity Using Multiple Lines of Evidence. *Reviews of Geophysics*, 58(4). Retrieved from <https://onlinelibrary.wiley.com/doi/10.1029/2019RG000678> doi: 10.1029/2019RG000678
- Soden, B. J., Held, I. M., Colman, R., Shell, K. M., Kiehl, J. T., & Shields, C. A. (2008, 7). Quantifying Climate Feedbacks Using Radiative Kernels. *Journal of Climate*, 21(14), 3504–3520. Retrieved from <http://journals.ametsoc.org/doi/10.1175/2007JCLI2110.1> doi: 10.1175/2007JCLI2110.1
- Tierney, J. E., King, J., Osman, M. B., Abell, J. T., Burls, N. J., Erfani, E., ... Feng, R. (2025, 2). Pliocene Warmth and Patterns of Climate Change Inferred From Paleoclimate Data Assimilation. *AGU Advances*, 6(1). Retrieved from <https://agupubs.onlinelibrary.wiley.com/doi/10.1029/2024AV001356> doi: 10.1029/2024AV001356
- Zhu, J., Otto-Bliesner, B. L., Brady, E. C., Gettelman, A., Bacmeister, J. T., Neale, R. B., ... Kay, J. E. (2022, 4). LGM Paleoclimate Constraints Inform Cloud Parameterizations and Equilibrium Climate Sensitivity in CESM2. *Journal of Advances in Modeling Earth Systems*, 14(4), e2021MS002776. Retrieved from <https://onlinelibrary.wiley.com/doi/10.1029/2021MS002776> doi: 10.1029/2021MS002776